Published in final edited form as:
Nature. 2005 August 4; 436(7051): 725–730.

Crucial role of p53-dependent cellular senescence in suppression of Pten-deficient tumorigenesis

Zhenbang Chen[1,2], **Lloyd C. Trotman**[1,2], **David Shaffer**[1,3], **Hui-Kuan Lin**[1,2], **Zohar A. Dotan**[1,2], **Masaru Niki**[1,2], **Jason A. Koutcher**[3], **Howard I. Scher**[3], **Thomas Ludwig**[4], **William Gerald**[2], **Carlos Cordon-Cardo**[2], and **Pier Paolo Pandolfi**[1,2]

1 *Cancer Biology and Genetics Program, Memorial Sloan-Kettering Cancer Center, Sloan-Kettering Institute, 1275 York Avenue, New York, New York 10021, USA*

2 *Department of Pathology, Memorial Sloan-Kettering Cancer Center, Sloan-Kettering Institute, 1275 York Avenue, New York, New York 10021, USA*

3 *Departments of Medicine, Radiology and Medical Physics, Memorial Sloan-Kettering Cancer Center, Sloan-Kettering Institute, 1275 York Avenue, New York, New York 10021, USA*

4 *Department of Anatomy and Cell Biology, Institute of Cancer Genetics, Columbia University, 1150 St Nicholas Avenue, New York, New York 10032, USA*

Abstract

Cellular senescence has been theorized to oppose neoplastic transformation triggered by activation of oncogenic pathways *in vitro*[1–3], but the relevance of senescence *in vivo* has not been established. The PTEN and p53 tumour suppressors are among the most commonly inactivated or mutated genes in human cancer including prostate cancer[4,5]. Although they are functionally distinct, reciprocal cooperation has been proposed, as PTEN is thought to regulate p53 stability, and p53 to enhance *PTEN* transcription[6–10]. Here we show that conditional inactivation of *Trp53* in the mouse prostate fails to produce a tumour phenotype, whereas complete *Pten* inactivation in the prostate triggers non-lethal invasive prostate cancer after long latency. Strikingly, combined inactivation of *Pten* and *Trp53* elicits invasive prostate cancer as early as 2 weeks after puberty and is invariably lethal by 7 months of age. Importantly, acute *Pten* inactivation induces growth arrest through the p53-dependent cellular senescence pathway both *in vitro* and *in vivo*, which can be fully rescued by combined loss of *Trp53*. Furthermore, we detected evidence of cellular senescence in specimens from early-stage human prostate cancer. Our results demonstrate the relevance of cellular senescence in restricting tumorigenesis *in vivo* and support a model for cooperative tumour suppression in which p53 is an essential failsafe protein of *Pten*-deficient tumours.

‘Cellular senescence’ describes a permanent form of cell cycle arrest in primary cultured cells, which can be triggered by DNA damage or activated oncogenes[1–3]. Although it has been implicated in mediating the response to anti-tumour treatments[11], there is still no evidence that senescence opposes tumorigenesis.

Up to 70% of primary prostate tumours lose one *PTEN* allele and retain the other copy[12–15]. Similarly, p53 is found completely lost or mutated almost exclusively in advanced prostate cancer[16,17]. Because complete loss of *Pten* in the mouse seems to be crucial for the development of invasive prostate tumours[18,19], why human invasive prostate cancer would

Correspondence and requests for materials should be addressed to P.P.P. (p-pandolfi@ski.mskcc.org).

Supplementary Information is linked to the online version of the paper at www.nature.com/nature.

not also select for complete *PTEN*-loss is puzzling. Similarly, the observation that p53 is lost not at presentation but in advanced prostate cancer was surprising, because loss of p53 favours tumour initiation in many tissues. A network involving the mutual dependence of PTEN and p53 has emerged that could partly reconcile the paradox. Specifically, PTEN may protect p53 from Mdm2-mediated degradation, whereas p53 can enhance the transcription of PTEN[6–10]. Inactivation of either gene should result in lower protein levels of the other gene. Thus, a loss of *PTEN* or p53 could mimic two genetic hits in one. To test the relevance of these observations in a well-defined model for tumour progression, we generated mice in which the *Pten* and/or *Trp53* genes are deleted specifically in the prostate. This analysis led to unforeseen observations that contradict the above hypothesis and show the importance of cellular senescence for tumour suppression *in vivo*.

For prostate-specific inactivation, we made use of the Cre/*loxP* technique[20] and *Probasin-Cre4* (*Pb-Cre4*) transgenic mice expressing *Cre* after puberty (at age 7 weeks) in prostatic epithelium[21]. We obtained $Pten^{loxP/loxP}$;*Pb-Cre4* and $Trp53^{loxP/loxP}$;*Pb-Cre4* mice, hereafter referred to as $Pten^{pc-/-}$ and $Trp53^{pc-/-}$ (Supplementary Fig. S1). As expected, in the presence of *Pb-Cre4*, recombination of *Pten* and *Trp53* was restricted to the three prostatic lobes, namely the anterior prostate (AP), ventral prostate (VP) and dorsolateral prostate (DLP), with minor recombination occurring in seminal vesicles (Supplementary Fig. S2a).

To study early effects of *Pten* and/or *Trp53* inactivation in the prostate, mice were killed at 9 weeks of age and histopathological analysis was performed. Wild-type (WT) mice displayed normal prostate histology, whereas age-matched $Pten^{pc-/-}$ littermates consistently displayed high-grade prostatic intraepithelial neoplasia (HG-PIN) in all three prostate lobes (roughly 50–60% of prostate glands affected: $n = 10$; Fig. 1a and Supplementary Fig. S2b), showing early onset of tumorigenesis immediately after *Pten* excision. In $Trp53^{pc-/-}$ mice, no pathological changes (hyperplasia or PIN) were found in any prostate lobes, and their prostate glands were indistinguishable from age-matched WT mice ($n = 10$; Fig. 1b and Supplementary Fig. S2b). Up to 18 months (Supplementary Fig. S2c; not shown), there were no differences in morphology and no differences detected by immunostaining for androgen receptor (glandular epithelial marker) or p63 (basal cell marker) (Supplementary Fig. S2d).

In contrast, on combined inactivation of *Pten* and *Trp53*, we found HG-PIN in all three lobes from 100% of mice, and invasive prostate cancer in 50% of $Pten^{pc-/-}$;$Trp53^{pc-/-}$ mice by age 10 weeks ($n = 12$) (Fig. 1a, b and Supplementary Fig. S2b). By 11 weeks, invasive adenocarcinoma was restricted to $Pten^{pc-/-}$;$Trp53^{pc-/-}$ mutants (Fig. 1b) whereas $Pten^{pc-/-}$ animals presented with invasive prostate cancer after a 4–6-month latency. Thus, in contrast to loss of *Pten*, loss of *Trp53* does not initiate prostate tumours but accelerates the progression of tumours initiated by loss of *Pten*.

We followed a cohort of 128 mice over 10 months for survival analysis, with two-weekly magnetic resonance imaging (MRI) analyses[19]. None of the $Pten^{pc-/-}$ mutants died of prostate cancer (Fig. 1c), which is consistent with our previous study[19]. In contrast, reduction of *Trp53* in a *Pten*-null background markedly reduced survival in a dose-dependent manner (Fig. 1c). Notably, all $Pten^{pc-/-}$;$Trp53^{pc-/-}$ mice died by 7 months of age (mean survival 5 ± 0.5 months), probably due to bladder obstruction and renal failure. Distant metastases were not observed in these mice or in $Pten^{pc-/-}$ mice in a 2.5-year follow-up (ref. 19, and Z.C and P.P.P., unpublished observations). By 6 months, MRI revealed masses in $Pten^{pc-/-}$ prostates but not in $Trp53^{pc-/-}$ or wild-type prostates (Fig. 1d). The average tumour weight in double-null mice was increased 32-fold in comparison with tumours in $Pten^{pc-/-}$ mice (Fig. 1e, f) and tumours predominantly showed poorly differentiated histology (Supplementary Fig. S2c). Tumours arising in $Pten^{pc-/-}$;$Trp53^{pc-/-}$ mice encompassed the entire genitourinary tract and pelvis. In contrast, tumours in $Pten^{pc-/-}$ mice retained clearly distinguishable urogenital organ

boundaries. Thus, inactivation of *Trp53* leads to massive tumour growth and lethal prostate cancer, but only in combination with *Pten* deficiency.

We investigated the molecular basis of cooperation between *Trp53* and loss of *Pten* by using primary mouse embryonic fibroblasts (MEFs). To study the effect of acute inactivation of *Pten* and *Trp53* we infected MEFs with retroviruses expressing Cre-PURO-IRES conjugated with green fluorescent protein (GFP) (Fig. 2a and Supplementary Fig. S3a). Virus-mediated expression of Cre led to efficient recombination of loxP alleles and increased Akt activation (Supplementary Fig. S3a). *Pten* heterozygous ($Pten^{\Delta/+}$) MEFs proliferated more rapidly than *Pten* WT ($Pten^{+/+}$) MEFs, but the proliferation of *Pten*-null ($Pten^{\Delta/\Delta}$) MEFs was similar to that of the WT (Fig. 2a). *Pten*-null MEFs exhibited the distinctive morphology of senescent cells (flattened large cells; not shown) and were positive for senescence-associated β-galactosidase (SA-β-Gal), a hallmark of senescent cells[22] (Fig. 2a and Supplementary Fig. S5a). To determine whether senescence was related to the selection process or to retroviral integration, we made use of transient episomal delivery by means of adenovirus-Cre (Ad-Cre) infection. We found that the loss of one *Pten* allele resulted in accelerated growth compared with that of wild-type cells, yet the loss of both *Pten* alleles led to lower proliferation and high β-Gal staining (Supplementary Figs S3b, c and S5d). To ensure that these findings were unrelated to Cre activity, we attempted *Pten* knockdown by means of RNA interference (RNAi). A decrease in Pten levels by 50% in heterozygous MEFs did indeed result in lowered proliferation and senescence induction, confirming not only the Cre-independence of senescence, but also suggesting that acute loss of *Pten* below the heterozygosity threshold can elicit a cellular senescence response (Fig. 2b, and Supplementary Figs S3d and S5b).

Next we assessed the status of the p53 senescence pathway. Acute loss of *Pten* resulted in Akt activation and consistent induction of p53 levels (Fig. 2c) but not phosphorylation of p53 serine 15 (Supplementary Fig. S3f). Upregulation of p21 and the senescence marker plasminogen activator inhibitor-1 (PAI-1) was observed in *Pten*-deficient MEFs but not in *Pten*/*Trp53* double-null MEFs (Fig. 2c and Supplementary Fig. S3g). Furthermore, loss of *Trp53* led to a marked increase in proliferation in the *Pten*-null background (Fig. 2d and Supplementary Fig. S3e). In addition, SA-β-Gal activity in $Pten^{\Delta/\Delta}$ MEFs decreased sharply in a p53 dose-dependent manner and was undetectable in double-null MEFs. These findings confirm that escape from senescence is essential for $Pten^{\Delta/\Delta}$ MEFs to realize full proliferative potential (Fig. 2d). Staining by TdT-mediated dUTP nick end labelling (TUNEL) revealed no difference in apoptosis between *Pten*-null and *Pten*/*Trp53* double-null MEFs (2 and 4 days, not shown). Finally, we tested whether p53 antagonizes cellular transformation of MEFs[23]. Complete inactivation of *Pten* and *Trp53* resulted in transformation of MEFs, whereas transformation potential decreased in a *Pten* or *Trp53* copy-dependent manner (Fig. 2e). These findings suggested that a p53-mediated senescence response restricts cell growth after loss of *Pten*.

Next we investigated whether the stability of p53 was altered on loss of *Pten* as reported previously[9]. In fact, we observed a prolonged rather than a reduced half-life of p53 protein in *Pten*-null compared with WT MEFs (Fig. 3a). This could be explained by the fact that complete loss of *Pten* resulted in increased accumulation of $p19^{Arf}$ (Fig. 3b), which is implicated in both the induction of cellular senescence and p53 stabilization through Mdm2 inhibition[1,2]. $p16^{INK4a}$ protein levels were also increased (Fig. 3b). In particular we found that the half-life of p21 was prolonged (Fig. 3a), indicating that p53-independent (post-transcriptional) mechanisms might also affect the accumulation of p21. Nevertheless, p53 was essential for p21 induction, because p21 was almost undetectable in *p53*/*Pten* double-null cells (Fig. 2c). Moreover, as reported previously[24], an activated form of Akt (myristoylated Akt) elicited growth arrest and cellular senescence in primary MEFs, supporting the notion that senescence caused by acute loss of *Pten* is at least partly due to Akt activation (Fig. 3c and Supplementary Fig. S5c).

To determine whether these observations were relevant *in vivo* to prostate cancer we performed immunohistochemical analysis (IHC). Staining of Pten revealed that *Pten* was efficiently and specifically deleted and unaffected by *Trp53* status (Supplementary Fig. S4a). Akt activation and membrane recruitment were correlated only with loss of *Pten* in *Pten*$^{pc-/-}$ and *Pten*$^{pc-/-}$;*Trp53*$^{pc-/-}$ mice, and not with p53 status (Supplementary Fig. S4a). In parallel, frozen prostate sections were stained for β-Gal activity. Whereas *Pten*-null prostates contained large numbers of senescent cells (‘blue glands’), WT prostates had very few (Fig. 4a and Supplementary Fig. S6b). Quantification revealed a 20-fold increase in senescent epithelial cells at 11 weeks compared with WT (Fig. 4b), but senescent cells were markedly decreased in the double-null prostates (Fig. 4a, b and Supplementary Fig. S6b). In addition, no cellular senescence was detected after heterozygous inactivation of *Pten* in *Pten*$^{pc+/-}$ single or compound mutants (Supplementary Fig. S6a), which is consistent with our MEF results (Supplementary Fig. S5a, b, d) and in full agreement with the fact that partial or complete inactivation of *Trp53* did not accelerate the PIN phenotype of *Pten*$^{pc+/-}$ mutants (not shown). Apoptosis in prostates from various mutants remained comparable (Fig. 4c), whereas senescence of epithelial cells was accompanied by inverse changes in cellular proliferation (Fig. 4d); this was confirmed by double labelling of *Pten*-mutant and double mutant glands with Ki-67 and β-Gal (Supplementary Fig. S4b).

We next studied whether p53 is upregulated on *Pten* inactivation *in vivo*. Indeed, we found increased accumulation of p53 in the nuclei of prostate epithelial cells from *Pten*$^{pc-/-}$ mice but not from WT (or *Pten*$^{pc-/-}$; *Trp53*$^{pc-/-}$ mice (Fig. 4a). Lysates from *Pten*$^{pc-/-}$ prostates showed more than tenfold p53 induction by immunoblotting (Fig. 4e). Importantly, p19^{Arf} and p21 protein levels were also increased in *Pten*$^{pc-/-}$ mice (Fig. 4a), confirming *in vivo* activation of the p19^{Arf} →p53 → p21 senescence pathway.

To address the relevance of these findings to human cancer we stained for senescence in specimens from early-stage human prostate cancer (n = 12; Supplementary Table S1). Strongβ-Gal staining was observed specifically in regions of prostate hyperplasia/PIN in some glands (3 of 12 samples, magnification × 100), but never in areas of frank tumour. Weak staining was observed in a further four samples at higher magnification (× 400), predominantly in areas of prostate hyperplasia/PIN and rarely in areas of carcinoma (Fig. 4f; Supplementary Table S1).

Prostate cancer, the second leading cause of cancer-related deaths in males (after lung cancer), strikes one in six men in the USA[25,26] and involves alterations of multiple tumour suppressor genes[27]. Our data provide insight into the molecular relationship between Pten and p53 in the prostate by demonstrating that loss of *Pten* induces p53 function (Fig. 4g). Because it has remained unclear whether loss of p53 function is associated with the initiation or progression of prostate cancer, our data firmly associate loss of *Trp53* with a crucial role in prostate cancer progression (Fig. 4h). Our results show that acute loss of *Pten* does not result in decreased, but increased, p53 levels and function. Conversely, loss of *Trp53* has no effect on Pten expression *in vitro* and in prostatic epithelium, whereas in combination with loss of *Pten* a lethal acceleration of prostate cancer is observed. Thus, regarding the Pten–p53 network, our data lend no support to a ‘two-in-one’ hit model of tumorigenesis, but as both genes need to be ablated for maximal disease progression they suggest a ‘one-by-one’ hit model for the genetic interaction of these major tumour suppressor genes. Our findings have therapeutic implications, because they indicate that *PTEN*-deficient prostate cancer might benefit from drugs that potentiate p53 activation in favour of a cellular senescence programme[28,29] (Fig. 4g). The fact that acute homozygous (not heterozygous) loss of *Pten* triggers a p53-dependent cellular senescence programme *in vivo* provides a plausible explanation for why human prostate cancer at presentation does not select for complete loss of *PTEN* and thus highlights the relevance of PTEN haploinsufficiency for prostate cancer initiation. Furthermore, the finding that complete

p53 inactivation alone has no phenotypic consequences in prostate could explain why loss of *p53* is preferentially selected for in advanced prostate cancer where in addition it could allow the tumour to reach maximal proliferation through *PTEN* loss of heterozygosity.

METHODS

Pten and *Trp53* mutant mice

Pten$^{loxP/loxP}$ mice were generated as described previously[19], and *Trp53*$^{loxP/loxP}$ mice were generated with a similar strategy (Supplementary Fig. S1; details are available from the authors). Female *Pten*$^{loxP/loxP}$;*Trp53*$^{loxP/loxP}$ mice were crossed with male *PB-Cre4* transgenic mice[21] for the prostate-specific deletion of *Pten* and *Trp53*. For genotyping, tail DNA was subjected to polymerase chain reaction analysis with the following primers. For *Pten*$^{loxP/loxP}$, primer 1 (5′-AAAAGTTCCCCTGCTGATGATTTGT-3′) and primer 2 (5′-TGTTTTTGACCAATTAAAGTAGGCTGTG-3′) were used. To detect the deleted allele, Lpten3 primer (5′-TTCTCTTGAGCA CTGTTTCACAGGC-3′) and primer 1 were used. For *Trp53*$^{loxP/loxP}$, primer 1 (5′-GAGACGCTGAGTCCGGTTCCCTCC-3′) and primer 2 (5′-GCAAGA GGTGACTTTGGGGTGAAGCTC-3′) were used.

Constructs

pMSCV-Cre-PIG was constructed by subcloning *Cre* into pMSCV-PURO-IRES-GFP (MSCV-PIG) vector (a gift from S. W. Lowe). The Nuclear Localization Sequence fusion Cre recombinase (NLS-Cre) was excised from pTZ-CreN vector (a gift from L. Nitschke).

Cell proliferation, transformation, senescence and apoptosis assays

Primary MEFs were prepared as described previously from individual embryos of various genotypes[30], and infected with retroviruses expressing Cre-PURO-IRES-GFP, myristoylated Akt (mAkt) or corresponding control viruses. To prepare retro-viral particles, 2×10^6 Phoenix cells were plated per 10-cm culture dish, and then pMSCV-Cre-PURO-IRES-GFP or empty vector was transfected with Lipofectamine 2000 (Invitrogen). For infection, MEFs at passage 2 were plated at a density of (3–4) $\times 10^5$ cells per 10-cm culture dish and infected by virus from Phoenix cells 48 h after transfection. After selection in the presence of 3μg ml^{-1} puromycin (Sigma), MEFs at passage 6 were used for growth curves, western blotting and senescence analysis. To determine senescence, MEFs were plated at 10^4 cells per well of a six-well plate in triplicate, and after 4 days SA-β-Gal activity was revealed with the senescence detection kit (Calbiochem) and quantified (more than 200 cells per sample). For prostate tissue, frozen sections 6μm thick were stained for β-Gal as above. For transformation assay, selected MEFs (3×10^4) at passage 6 were suspended in medium containing 0.3% agar onto solidified 0.6% agar per well of a six-well plate, and the number of colonies was assessed after 21 days. For apoptosis analysis, dewaxed and rehydrated paraffin sections were treated for with the *in situ* Cell Death Detection Kit (Roche). Apoptotic cells were identified by positive TUNEL staining. A total of 500 cells were counted from five different fields for each section, and the analysis was repeated at least twice for each genotype.

Short hairpin RNA (shRNA)

Pten-directed shRNA (5′-GATCCCCAGACCA TAACCCACCACAGTTCAAGAGACTGTGGTGGGTTATGGTCTTTTTTA-3′) was designed using the Oligoengine RNAi design tool; the resulting oligonucleotides were subcloned into the pSUPER-puro vector (Oligoengine) and trans-fected into Phoenix packaging cells. The random oligonucleotide (5 ′-GATCCCCAAGGAGACGAGCAAGAGAATTCAAGAGATTCTCTTGCTCGTC TCCTTTTTTTA-3′) was used as control. Primary *Pten* WT or heterozygous MEFs at passage

2 were infected, selected (3 days in 2μg ml^{-1} puromycin) and plated at 2.5×10^4 cells per well in 12-well dishes in duplicates for determination of growth curves by spectroscopic measurement of crystal violet uptake. β-Gal activity was measured on day 4 of the growth curve with cells treated identically and in parallel.

Western blot and immunohistochemistry

MEF lysates were prepared with RIPA buffer (1 × PBS, 1% Nonidet P40, 0.5% sodium deoxycholate, 0.1% SDS and protease inhibitor cocktail (Roche)). The following antibodies were used for western blotting: mouse monoclonal anti-Pten (6H2.1; Cascade BioScience), rabbit polyclonal anti-$p19^{Arf}$ (Ab-1; Calbiochem), rabbit polyclonal anti-p53 (CM5; Novocastra), rabbit polyclonal anti-Akt and anti-phosphoserine 473 of Akt (Cell Signalling), rabbit polyclonal anti-p21 (C-19; Santa Cruz), rabbit polyclonal anti-p16 (M-156; Santa Cruz), rabbit polyclonal anti-PAI-1 (H-135; Santa Cruz) and mouse monoclonal anti-β-actin (AC-74; Sigma). To determine p53/p21 protein half-life, MEFs ($Pten^{+/+}$-*Cre* and $Pten^{\Delta/\Delta}$ -*Cre*, at 80% con-fluence and equal passage number) were treated with 30μg ml^{-1} cycloheximide (Sigma) and harvested at the indicated times for western blot analysis. For prostate analysis, protein extracts were prepared by grinding prostate tissues in RIPA buffer at a ratio of 1 mg per 5μl. After brief sonication and centrifugation, the supernatant was collected for western blotting. Antibodies used were rabbit polyclonal anti-PTEN (9552; Cell Signalling). Antibodies against p53, pAkt and Akt were as above. For immunohistochemistry (IHC), tissues were fixed in 10% formalin and embedded in paraffin in accordance with standard procedures. Sections were stained for phospho-Akt (Ser 473) antibody (Cell Signalling), PTEN (Ab-2; NeoMarkers), Ki-67 (Novocastra), $p19^{Arf}$ (ab80-50; Abcam), p21 (F-5; Santa Cruz), p53 (FL-393; Santa Cruz), androgen receptor (N-20; Santa Cruz) and p63 (550025; Becton Dickson Transduction Lab).

MRI

Individual mice were subjected to MRI assessment for the detection of prostate tumours. In brief, mice were anaesthetized with 2% isofluorane, and images were obtained on a Bruker 4.7-T 40-cm bore magnet with a commercial 7-cm inner diameter birdcage coil similar to the protocol described previously[19]. Low-resolution sagittal and axial scout images were obtained initially, followed by high-spatial-resolution T_2-weighted axial images (repetition interval (T_R) = 3,800 ms, effective echo time (T_E) = 35 ms, eight echoes per phase encoding step, spatial resolution = 1.0 mm slice thickness × 112μm × 112μm in plane resolution, and four repetitions of data acquisition for 8–9 min of imaging time). Invasiveness-free and cumulative survival curves were obtained with Kaplan–Meier analysis as described previously[19].

Supplementary Material

Refer to Web version on PubMed Central for supplementary material.

Acknowledgements

We thank T. Maeda and T. Jacks for helpful suggestions; D. Peeper, C. Schmitt and M. Serrano for exchanging unpublished data and coordinating the submission of manuscripts; N. Hay, U. Greber and S. Hemmi for reagents; L. Cai and L. DiSantis for critical reading and editing of the manuscript; other members of the Pandolfi lab for advice and discussion; K. Manova and C. Farrell from the Molecular Cytology Core Facility for assistance with IHC analysis; and C. Le, C. Matei, D. Procissi and I. Buchanan for MRI analysis. This work was supported by NIH grants to P.P.P.

References

1. Lowe SW, Cepero E, Evan G. Intrinsic tumour suppression. Nature 2004;432:307–315. [PubMed: 15549092]

2. Serrano M, Blasco MA. Putting the stress on senescence. Curr Opin Cell Biol 2001;13:748–753. [PubMed: 11698192]
3. Campisi J. Cellular senescence as a tumour-suppressor mechanism. Trends Cell Biol 2001;11:S27–S31. [PubMed: 11684439]
4. Vogelstein B, Lane D, Levine AJ. Surfing the p53 network. Nature 2000;408:307–310. [PubMed: 11099028]
5. Di Cristofano A, Pandolfi PP. The multiple roles of PTEN in tumour suppression. Cell 2000;100:387–390. [PubMed: 10693755]
6. Stambolic V, et al. Regulation of PTEN transcription by p53. Mol Cell 2001;8:317–325. [PubMed: 11545734]
7. Mayo LD, Donner DB. A phosphatidylinositol 3-kinase/Akt pathway promotes translocation of Mdm2 from the cytoplasm to the nucleus. Proc Natl Acad Sci USA 2001;98:11598–11603. [PubMed: 11504915]
8. Zhou BP, et al. HER-2/neu induces p53 ubiquitination via Akt-mediated MDM2 phosphorylation. Nature Cell Biol 2001;3:973–982. [PubMed: 11715018]
9. Freeman DJ, et al. PTEN tumour suppressor regulates p53 protein levels and activity through phosphatase-dependent and -independent mechanisms. Cancer Cell 2003;3:117–130. [PubMed: 12620407]
10. Trotman LC, Pandolfi PP. PTEN and p53: who will get the upper hand? Cancer Cell 2003;3:97–99. [PubMed: 12620402]
11. Schmitt CA, et al. A senescence program controlled by p53 and p16INK4a contributes to the outcome of cancer therapy. Cell 2002;109:335–346. [PubMed: 12015983]
12. Suzuki H, et al. Interfocal heterogeneity of PTEN/MMAC1 gene alterations in multiple metastatic prostate cancer tissues. Cancer Res 1998;58:204–209. [PubMed: 9443392]
13. Feilotter HE, Nagai MA, Boag AH, Eng C, Mulligan LM. Analysis of PTEN and the 10q23 region in primary prostate carcinomas. Oncogene 1998;16:1743–1748. [PubMed: 9582022]
14. Muller M, Rink K, Krause H, Miller K. PTEN/MMAC1 mutations in prostate cancer. Prostate Cancer Prostatic Dis 2000;3:S32. [PubMed: 12497140]
15. Hermans KG, et al. Loss of a small region around the PTEN locus is a major chromosome 10 alteration in prostate cancer xenografts and cell lines. Genes Chromosom Cancer 2004;39:171–184. [PubMed: 14732919]
16. Qian J, et al. Loss of p53 and c-myc overrepresentation in stage T(2–3)N(1–3)M(0) prostate cancer are potential markers for cancer progression. Mod Pathol 2002;15:35–44. [PubMed: 11796839]
17. Navone NM, et al. p53 mutations in prostate cancer bone metastases suggest that selected p53 mutants in the primary site define foci with metastatic potential. J Urol 1999;161:304–308. [PubMed: 10037428]
18. Di Cristofano A, De Acetis M, Koff A, Cordon-Cardo C, Pandolfi PP. Pten and $p27^{KIP1}$ cooperate in prostate cancer tumour suppression in the mouse. Nature Genet 2001;27:222–224. [PubMed: 11175795]
19. Trotman LC, et al. Pten dose dictates cancer progression in the prostate. PLoS Biol 2003;1:385–396.
20. Jonkers J, Berns A. Conditional mouse models of sporadic cancer. Nature Rev Cancer 2002;2:251–265. [PubMed: 12001987]
21. Wu X, et al. Generation of a prostate epithelial cell-specific Cre transgenic mouse model for tissue-specific gene ablation. Mech Dev 2001;101:61–69. [PubMed: 11231059]
22. Dimri GP, et al. A biomarker that identifies senescent human cells in culture and in aging skin *in vivo*. Proc Natl Acad Sci USA 1995;92:9363–9367. [PubMed: 7568133]
23. Weinberg RA. The cat and mouse games that genes, viruses, and cells play. Cell 1997;88:573–575. [PubMed: 9054495]
24. Miyauchi H, et al. Akt negatively regulates the *in vitro* lifespan of human endothelial cells via a p53/p21-dependent pathway. EMBO J 2004;23:212–220. [PubMed: 14713953]
25. Stewart SL, King JB, Thompson TD, Friedman C, Wingo PA. Cancer mortality surveillance—United States, 1990–2000. MMWR Surveill Summ 2004;53:1–108. [PubMed: 15179359]

26. Levi F, Lucchini F, Negri E, Boyle P, La Vecchia C. Leveling of prostate cancer mortality in Western Europe. Prostate 2004;60:46–52. [PubMed: 15129428]

27. Abate-Shen C, Shen MM. Molecular genetics of prostate cancer. Genes Dev 2000;14:2410–2434. [PubMed: 11018010]

28. Bykov VJ, et al. Restoration of the tumour suppressor function to mutant p53 by a low-molecular-weight compound. Nature Med 2002;8:282–288. [PubMed: 11875500]

29. Vassilev LT, et al. *In vivo* activation of the p53 pathway by small-molecule antagonists of MDM2. Science 2004;303:844–848. [PubMed: 14704432]

30. Maeda T, et al. Role of the proto-oncogene *Pokemon* in cellular transformation and *ARF* repression. Nature 2005;433:278–285. [PubMed: 15662416]

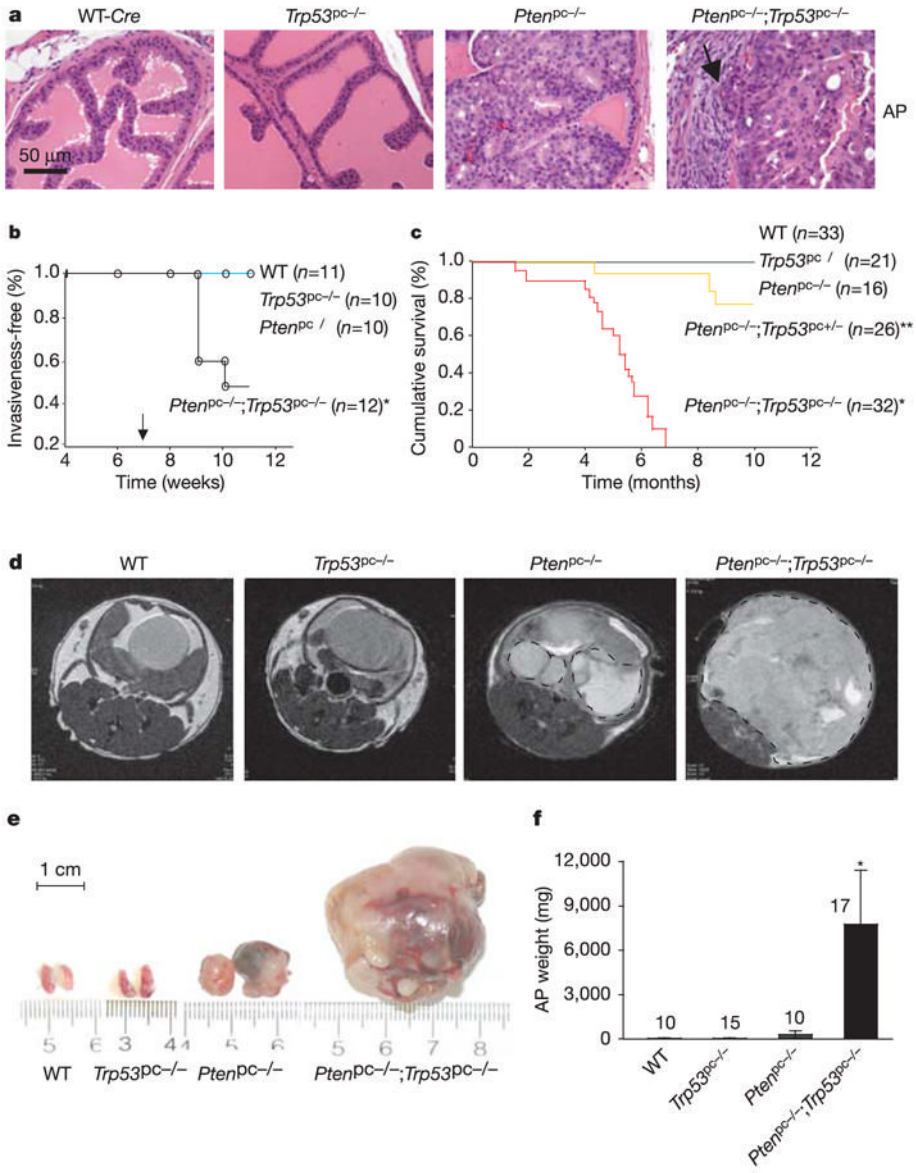

Figure 1. Loss of *Trp53* does not initiate prostate tumours but renders *Pten*-deficient carcinomas lethal

a, Histopathological analysis (haematoxylin/eosin staining) of anterior prostates (AP) in WT, *Pten* and *Trp53* single and double mutants at 9 weeks of age reveals normal glands in WT and *Trp53*$^{pc-/-}$ mice but PIN lesions in *Pten*$^{pc-/-}$ mice and invasion (arrow) in *Pten*$^{pc-/-}$;*Trp53*$^{pc-/-}$ mice. **b**, Disease-free survival curve (Kaplan–Meier plot) for prostate cancer. Adenocarcinoma was found only in the *Pten*$^{pc-/-}$;*Trp53*$^{pc-/-}$ cohort ($P < 0.05$). The arrow indicates puberty. **c**, Cumulative survival analysis. A statistically significant decrease in lifespan ($P < 0.0001$) compared with the *Pten*$^{pc-/-}$ cohort was found for the *Pten*$^{pc-/-}$;*Trp53*$^{pc-/-}$ cohort (asterisk) and for the *Pten*$^{pc-/-}$;*Trp53*$^{pc+/-}$ cohort (double asterisk). **d–f**, MRI of AP tumours (dashed circles) at 23–31 weeks (**d**) and their actual sizes (**e**) and weights (**f**) after biopsy. Error bars in **f** indicate s.d. of AP weight for the numbers of mice indicated above the bars.

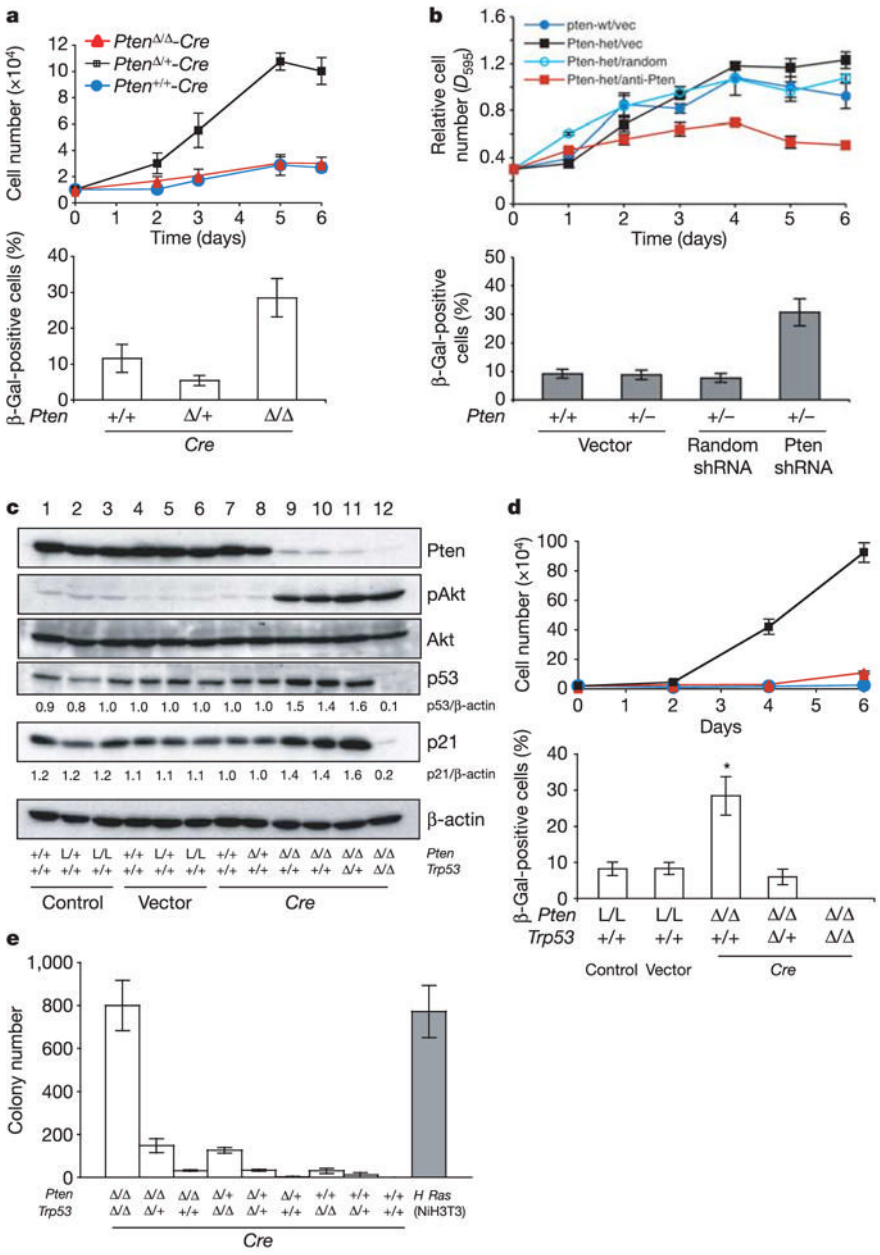

Figure 2. Acute loss of *Pten* triggers the p53-dependent senescence pathway in primary mouse embryonic fibroblasts (MEFs)

a, Top: growth curves of primary MEFs, infected with retroviral Cre (with selection) and followed over a 6-day period. Bottom: cellular senescence assay of cells from **a. b**, Top: growth curves of primary MEFs infected with Pten shRNA (with selection) and followed over a 6-day period. Bottom: cellular senescence assay of cells from **b. c**, Western blots of MEF lysates. Numbers indicate densitometrically determined protein levels relative to β-actin. **d**, Growth curves (top) and senescence staining (bottom) of $Pten^{\Delta/\Delta}$;$Trp53^{\Delta/\Delta}$ double-null MEFs (black squares), $Pten^{\Delta/\Delta}$;$Trp53^{\Delta/+}$ MEFs (red triangles) and $Pten^{\Delta/\Delta}$ MEFs (blue circles). Error bars indicate s.d. *L/L* indicates $Pten^{loxP/loxP}$. **e**, Transformation assay of all combinations of *Pten* and *Trp53* inactivation. H-Ras-infected NIH 3T3 cells served as positive control (grey bar). Error bars indicate s.d. for a representative experiment performed in triplicate.

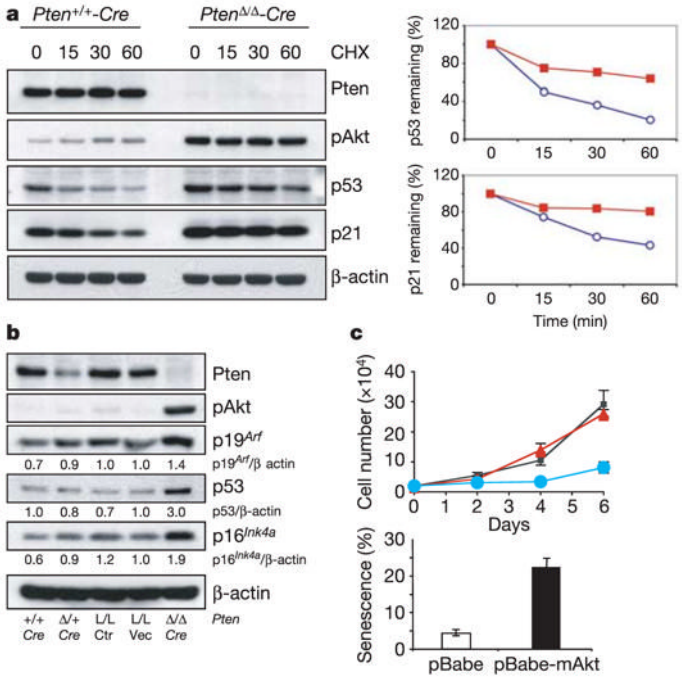

Figure 3. Acute loss of *Pten* results in ARF upregulation and p53/p21 stabilization in primary MEFs

a, Left: inhibition of protein synthesis by cycloheximide (CHX) and western blotting at the indicated times (minutes) shows that the half-life of p53 and p21 proteins is prolonged on acute loss of Pten in MEFs. Right: quantification of p53 and p21 half-life from the western blots, normalized to β-actin. Blue circles, *Pten*$^{+/+}$-*Cre*; red squares, *Pten*$^{\Delta/\Delta}$-*Cre*. **b**, Western blotting demonstrates upregulation of p19^{Arf} protein after acute *Pten* loss in MEFs. *Pten*$^{+/+}$-*Cre*, *Pten*$^{\Delta/+}$-*Cre*, *Pten*$^{loxP/loxP}$ (L/L, Ctrl) and *Pten*$^{loxP/loxP}$-MSCV vector (Pten$^{L/L}$-vec) serve as controls. **c**, Expression of myristoylated Akt (mAkt) in MEFs induces growth arrest (top) and cellular senescence (bottom). Black squares, control; red triangles, pBabe; blue circles, pBabe-mAkt. Error bars represent s.d. for a representative experiment performed in triplicate.

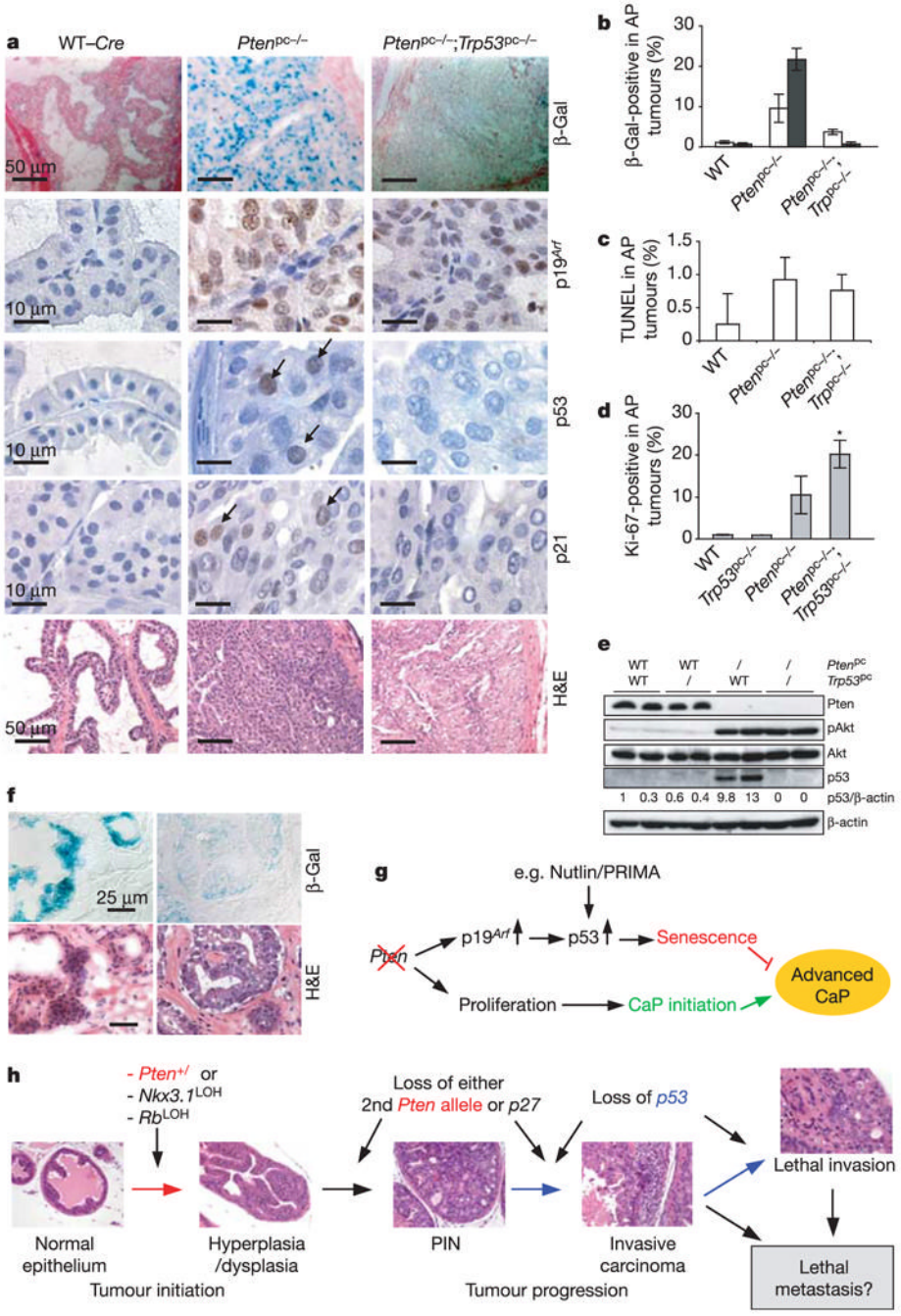

Figure 4. The p53-dependent cellular senescence pathway restricts tumorigenesis in *Pten*-deficient prostates

a, Senescence and histopathological analysis of 11-week-old prostates, stained as indicated. H&E, haematoxylin/eosin. Scale bars, 50μm (β-Gal and haematoxylin/eosin stain) and 10μm (p53, p19^{Arf} and p21). **b**, Quantification of the β-Gal staining seen on AP sections at 8 weeks (open bars) and 11 weeks (filled bars). Representative sections from three mice were counted for each genotype. **c**, Quantification of TUNEL assay for apoptosis in the AP at 11 weeks (of more than two mice per genotype). **d**, Quantification of Ki-67 staining of 11-week-old AP done as in **b.** Error bars in **b**–**d** represent s.d. for a representative experiment performed in triplicate. Asterisk indicates statistical significance between *Pten*$^{pc-/-}$ and *Pten*$^{pc-/-}$;*Trp53*$^{pc-/-}$ double

mutants ($P < 0.05$). **e**, Western blot analysis of AP tissue from each genotype at 11 weeks shows Akt activation and p53 induction in *Pten*$^{pc-/-}$ mice. **f**, Senescence (β-Gal) and histopathological (haematoxylin/eosin stain) analysis of cryosections from human radical prostatectomy samples, showing strong (+++) β-Gal staining from a hyperproliferative (preneoplastic) prostate gland (left) or weak (+) β-Gal staining from a neoplastic gland from a different patient (right). Scale bars, 25μm. **g**, A model for *Pten*-deficient tumorigenesis, p53 cooperativity and its therapeutic implications. *Pten*-deficient tumours may benefit from treatment with drugs that restore the activity of mutated p53 (for example, PRIMA[28]) or that stabilize WT p53 through the inactivation of MDM2 (for example, Nutlin[29]). **h**, A model for prostate tumour initiation, development and progression synergistically contributed by *Pten*, *Trp53* and other genes. Loss of Trp53 accelerates cancer progression by a senescence escape mechanism in *Pten*-deficient tumours.